Oxidized structure and Compositional properties of 1144 phase FBS by analytical electron microscopy

Z-H Sung[1*], A Masi[2*], JY Lee[1], A Duchenko[2,4], X Hu[3], A G Kim[5], and G Celentano[3]

[1]Fermi National Accelerator Laboratory, Batavia, IL, USA
[2].ENEA, C.R. Frascati, Via Enrico Fermi, 45, 00044 Frascati, Italy
[3]Northwestern University's Atomic and Nanoscale Characterization Experiment Center (NUANCE), Northwestern University, Evanston, IL, USA
[4]Università degli Studi RomaTre, Dipartimento di Ingegneria, Via Vito Volterra, 62, 00146 Roma, Italy
[5]Asia Pacific International School, Seoul, 01874, South Korea

E-mail: zsung@fnal.gov, andrea.masi@enea.it

Abstract. The 1144 phase (Ae1A1Fe4As4) shows a strong advantage of engineering fabrication among Fe (Iron)-based superconductor (FBS) family due to the robustness of its superconducting properties with respect to chemical inhomogeneities, granted by its uniform crystalline-layered structure. This regularity is furthermore associated to crystalline defects capable of acting as efficient pinning centers, from which high critical currents can achieved at high fields. Like other FBS phases, its lossless current-carrying capability can be remarkably degraded by distractions at grain boundaries (GBs). GB oxidation is an issue of upmost importance to the realization of the practical FBS application for high field (> 20T) magnet. In this study, we explore oxidized grain boundary and intrinsic grain structural properties of 1144 polycrystalline samples by applying analytical electron microscopy such as atomic resolution scanning transmission electron microscopy and atom probe tomography. These structural properties of samples produced by a mechanochemically assisted synthesis are evaluated following the degradation of superconducting properties due to oxidation. We observe a strong correlation between the contamination at grain boundaries and the decrease of transport properties of the bulk sample, while the crystallin structure seems to be not affected by the oxidation.

1. Introduction

Fe (iron)-based superconductor (FBS or iron pnictide), discovered in 2008 [1], is a promising material for superconducting wire technology applied for ultra-high field (>20 T) magnet [2]. It also has a significant advantage on cost reduction [3] because the superconductors itself are the main cost enabler for magnet fabrication. Recently developed processes have made significant improvement on suppression of extrinsic intergranular property like gran boundary weak-link problem with modification of FBS core texture [4, 5] and by applying the secondary thermal treatment in high purity environment [6]. FBS in a short wire (~100 m) form showed exceeded transport critical current density, J_c, close to 1.5 $\times$ 10^5 A/cm^2, at 4.2 K and 10 T [7].

The most easily scalable method of fabricating FBS wire is the Powder In Tube (PIT) technology [8]. Among FBS family, the Ca/K-1144 compound ($A_1AE_1Fe_4As_4$ chemical composition; A=Alkaline and AE= Alkaline-Earth) is composed by cheap and abundant elements, making this material a strong candidate to produce wires and tapes easily. Although the 122 ($A_xAE_{1-x}Fe_2As_2$) family have attracted most of the interest, showing the best performance and easiness of production [7], the 1144 family [9]

Content from this work may be used under the terms of the Creative Commons Attribution 4.0 licence. Any further distribution of this work must maintain attribution to the author(s) and the title of the work, journal citation and DOI.
Published under licence by IOP Publishing Ltd

constitutes a relatively novel class of FBS characterized by critical temperature of approximately 35 K and its intrinsic defect structure between uniform crystalline layers enables to promote high critical current densities in single crystalline compounds [9].

The developed mechanochemically assisted synthesis route [10] allowed to form polycrystalline Ca/K-1144 compounds composed of sub-micro-meter scale grains. This feature produces a dense network of boundaries between polycrystalline aggregates, as a result degrading the capability of delivering superconducting current [2,6]. In this work we submit the material to different oxidative conditions and explore the effect on the compound by assessing micro-structural variation in sub-atomic level though advanced analytical electron microscopy and atom probe tomography.

2. Experimental procedure

The 1144 compounds were synthesized in the same fashion of our previous works [11] by exploiting a mechanochemical step followed by a thermal treatment at 700°C. An average volumetric density of 4.1 g/cm^3 was obtained for the various pellets, corresponding to approximately a 79% density with respect to the theoretical value. But, we have not observed component deficient during the sintering like the 122 phase [12]. The sample were oxidized by exposition to the ambient air of an average humidity ratio of 3% with varying the exposure time.

Electric resistances were evaluated by conventional standard four-point transport measurement as a function of temperature. Specific heat capacities were obtained in a QD (quantum design) 14T PPMS (physical property measurement system) on small sample fragments by cooling down to 4K with and without an external applied magnetic field. Surface and cross-sectional microstructure were characterized with Thermofisher Helios 5 CX, dual beam system (field emission scanning electron microscope and Ga ion focused ion beam) in cooperation with Oxford Instrument, Xplore X-ray energy dispersive spectroscopy (EDS). Electron transparent foils were prepared for high resolution microstructural analysis by focused ion beam (FIB) using lift-out technique after capping the sample surface with a Pt protective layer. The atomic structure of the specimens were characterized by an aberration corrected JEOL ARM 200CF transmission electron microscope (TEM) and scanning-TEM. In addition, atomic level chemical compositions were acquired by 3D atom probe tomography and then compared with TEM/STEM with EDS. A tiny needle-shape specimen was prepared for APT by dual beam Helios 5CX as well.

3. Results

The oxidization effect on transport resistance of the Ca/K-1144 compounds are presented in Figure 1. The curves are reported in Figure 1(a), normalized at 273 K to highlight the different normal state behavior. The residual resistance ratio (RRR) at 40K (R_{273K}/R_{40K}) decreses with increasing air exposure. RRR values vary from values higher than 5.5 for fresh samples, to values lower than 2 for samples characterized by high degree of exposure, suggesting a general worsening of grain coupling and connectivity. However, at the low temperature region in Figure 1(b), the onset of the critical superconduting transition temperature, $T_{c,\ onset}$, does not vary with the period of the air exposure. This suggests that no disordering remained on the lattice of the 1144 compound grain even after long period of air exposure. $T_{c,\ onset}$ is the first deviation point from the linearity at high tempeature regime.

To evaluate oxidization phenomenon on the microstructure, the surface morphology of the 1144 compound is initially compared along with the air exposure time. The surface of a freshly synthesized compound is shown in Figure 2(a & c). Aggregates of the compound are densely distributed with open porosities. Interestingly, large crystals are easily observed on the surface. The aggregates are made of micro-meter scale crystalline. Different from the pristine, 3.5 weeks exposure caused edges of surface aggregates to be rounded, as shown in Figure 2(c & d). The bulk structural evolution was assessed by observing the cross section of the same pristine after exposure to air for 3.5 weeks. Figure 3 compares SEM section images and EDS maps of potassium (K), oxygen (O), and calcium (Ca) on the compound. The cross section of the pristine 1144 compound opened by FIB (Figure 3a) was slightly further milled (~ 50 nm) after 3.5 weeks exposure (Figure 3b) in order to get rid of oxidized surface layer. This process clearly revealed hided oxidization at the boundary between aggregates, indicated by high oxygen signals

as marked with a white arrow. This suggests that the sample surface evenly oxidize, and that oxygen diffuses into the bulk through preferential pathway like the boundaries of dense aggregates.

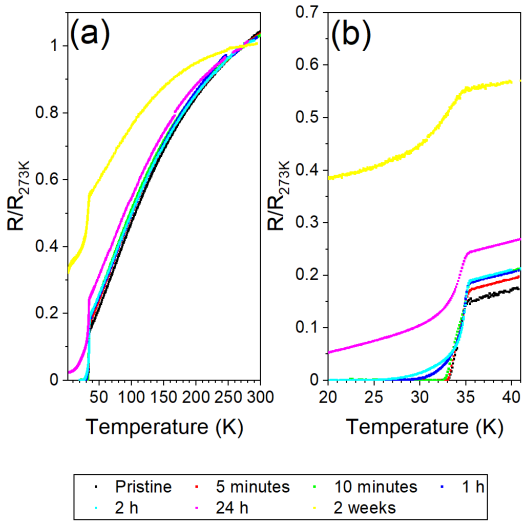

Figure 1. Resistance as a function of temperature for samples subjected to different air exposure (a) and enlarged view of the superconducting transition (b) (a reproduction of the reference [11]].

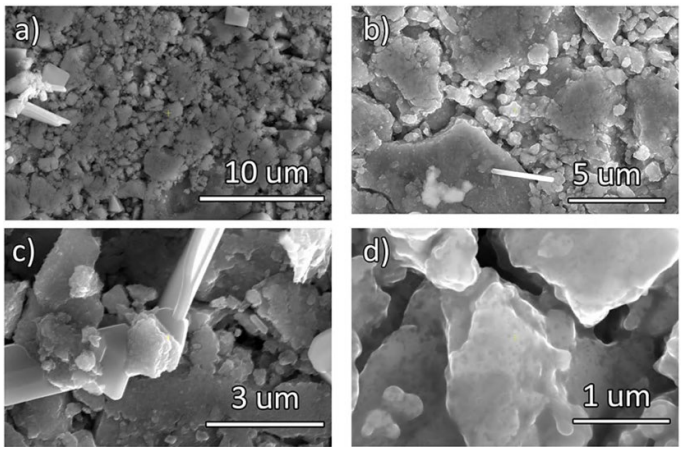

Figure 2. Secondary electron SEM image of the samples at the pristine (a & c) and after 3.5 weeks of air exposure (b & d).

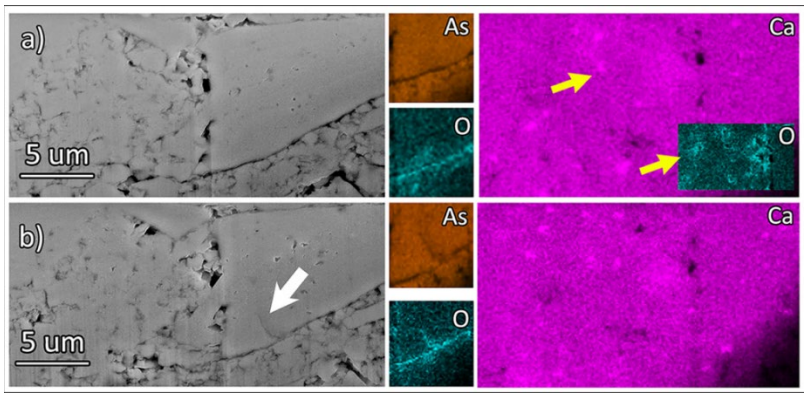

Figure 3. Secondary electron SEM images and EDS element maps of potassium (K), oxygen (O) and Ca (calcium) on the sample cross section. (a) the pristine condition, and (b) after 3.5 weeks of air exposure. White and yellow arrows indicate aggregate boundary and Ca-O precipitates, respectively.

For detailed microstructural analysis, thin lamellae were extracted from the bulk of the 3.5 weeks air exposed sample by FIB and examined by means of SEM/EDS as shown in Figure 4. This analysis allowed in fact to enhance the spatial resolution of EDS element characterizations, avoiding the bulk contribution to the EDS signals. Secondary electron through-the-lens (TLD) SEM image (Figure 4a) shows chemical compositional signals of electrons from the lamella, which are depicted similar to the EDS element maps (Figure 4c and 4d). Electron forwarded scattered SEM image discriminates grain boundary segregations from the 1144 stoichiometric grains. Figure 4d is a localized EDS map on a boundary of aggregates, indicating preferential oxide segregation along the aggregate boundaries. Ca (calcium) also locally precipitates with oxygen between the aggregates, similar to Figure 3. Small particles on the lamella surface (Figure 4a) are likely nano-meter size Ca oxide precipitates as shown in the TEM analysis as follow.

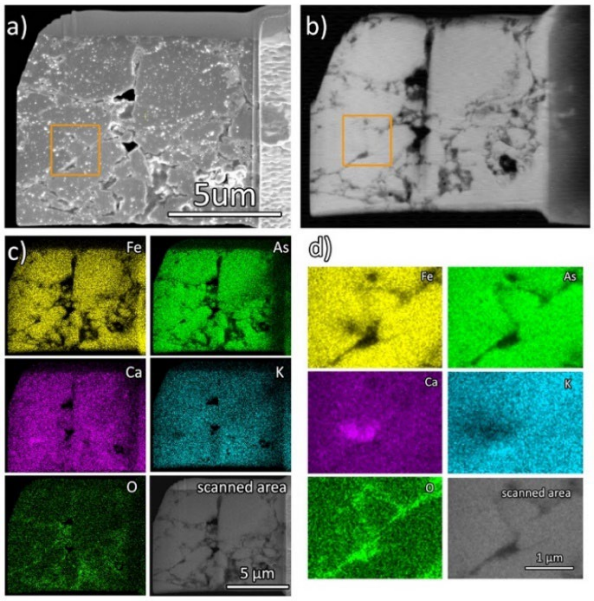

Figure 4. a) Secondary electron through-the-lens (TLD) and b) electron forward scattered SEM image on the cross-sectional surface of the compound after the 3.5 weeks air exposure, prepared by FIB. c) and d) are EDM mapping on elements.

The thin lamellae were further polished by FIB, and their detailed microstructures were characterized by TEM/STEM with EDS as shown in Figure 5 and 6. Staring from the low magnification image (Figure 5a), significant amounts of well-evident clear grain boundaries across the sample are observed. The EDS element map (Figure 5d) confirms that the white particles are Ca oxides. Based on high magnification bright field (BF) and dark field (DF) scanning transmission electron microscopy (STEM) images, it is estimated that thick (few tens of nano-meter) and thin (few nano-meter) boundaries are referred to the boundaries between aggregates and intrinsic grain boundaries, respectively. Obviously, the compound is formed by elongated grains of homogenous dimension, few tens of nano-meters on the short side and 100-200 nm along the long direction. Ca oxide particles mainly lie on the thick boundaries.

Atomic lattice structure of the Ca/K 1144 compound was characterized on the neighbouring grain close to a think (~20 nm) boundary by high angle angular dark field (HAAD) of STEM, as shown in Figure 6. Since a thick boundary is likely located between the aggregates, it was expected that atomic structures of the intrinsic 1144 grains would be disturbed by 3.5 weeks air oxidization. However, Figure 6c) shows the lattice structure is intact and highly ordered, which is composed of stacking of Fe, As, Ca, and K layers along [001] direction.

In addition, atomic resolution chemical composition of the compound was characterized by atom probe tomography. The line profile on the slice from the 3D reconstruction map presents high oxygen contents with suppression of iron (Fe) and arsenic (As) signals, which should be grain boundaries, similar to the TEM/STEM + EDS analysis.

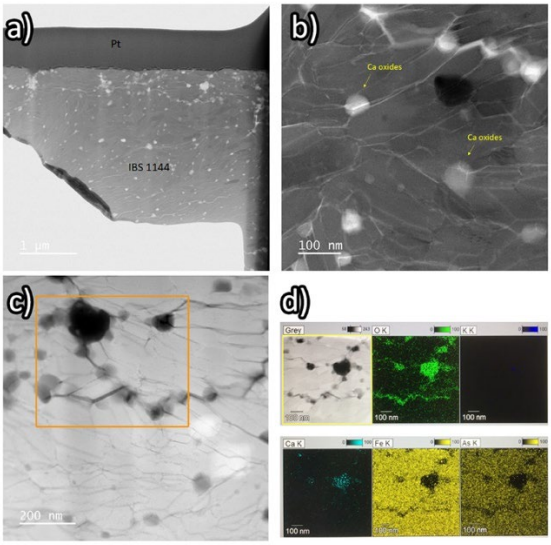

Figure 5. a) Low magnification bright field-transmission electron microscopy (BF-TEM), b) BF (bright field), c) DF (dark field)-scanning TEM images, and d) EDS maps on the area indicated by an orange square in c)

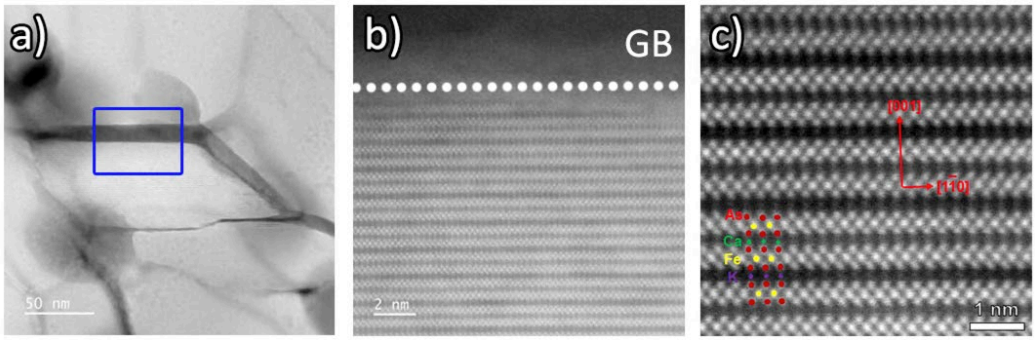

Figure 6. a) DF STEM image, b) high magnification STEM image near the thick grain boundary indicated by a blue square, a white line indicates a grain boundary, and c) atomic resolution high-angle annular dark-field (HAADF) image with the index of the 1144 FBS atomic structure.

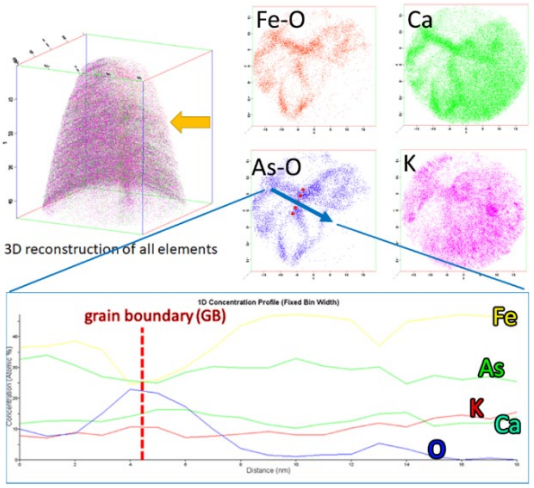

Figure 7. 3D atom probe tomography on the Ca/K 1144 compound after 3.5 weeks ambient air exposure. Top left) the 3D reconstruction for all elements, top right) element maps on the sliced surface as indicated by the orange arrow, and bottom) elements profile along the blue arrow.

The investigation of the superconducting properties of the compound by means of an appropriate intragrain technique such as the measurement of specific heat capacity is highly recommended to assess if the whole superconducting compound is affected by the oxidation phenomenon, lead to a worsening of the intrinsic superconducting properties. Figure 8 shows the specific heat ($C/T = \gamma_n$) of the pristine sample near the normal to superconducting transition after 24 hours, and 3.5 weeks air exposure with or without external magnetic field. The C/T plots shows a sharp and clear onset near 35 K in the absence of magnetic field and slightly shifted to lower temperature when 10 T magnetic field is applied after 24 hours exposure. It is obvious that there is no significant effect of oxidization on the intragranular superconducting properties of the compound. However, C/T plots are slightly degraded after 3.5 weeks exposure, even though the onsets are not changed. The enhancement of specific heats with air exposure is associated with oxidized layers on the samples surface.

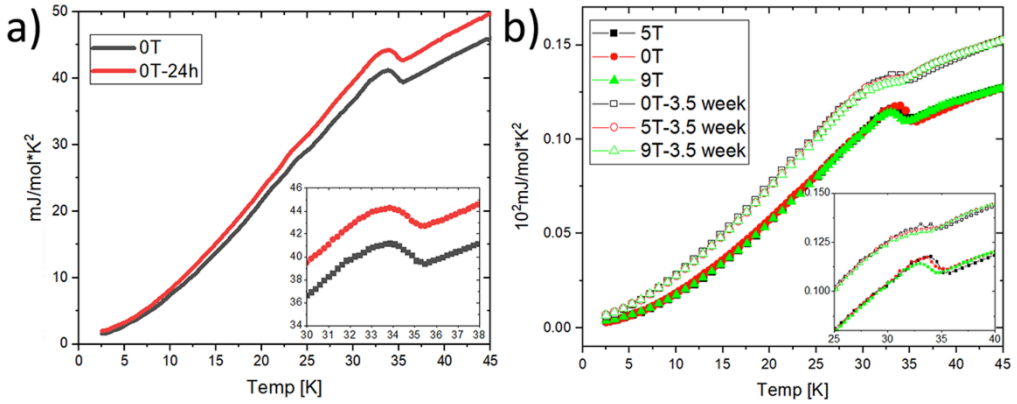

Figure 8. Volumetric specific heat capacity (C) of the Ca/K-1144 compound as a function of temperature with the ambient air exposure time (a) 24 hours and (b) 3.5 weeks. C/T vs T with an insert near T_c transition.

4. Summary and Conclusion

Weak link behavior at the grain boundaries of iron (Fe)-based superconductor (FBS) is the most vulnerable aspect that should be overcome to realize FBS wire technology for practical high field magnet application. Among FBS families [2], 122-phase has made a rapid progress toward to wire fabrication, achieving J_c, above 1.5×10^5 A/cm^2, at 4.2 K and 10 T [5,7,13]. Due to advantage of engineering fabrication associated with stoichiometric homogeneity from uniform superconducting crystalline structure, the Ca/K 1144 phase has recently attracted the most of interests. However, observing the evolution of this compound with respect to oxidation is imperative to transform the materials into a wire form.

In this study, we showed that the degradation of the superconducting properties is supposed to be due to granularity phenomena rather than to the decomposition of the superconducting compound, at least for the timescale investigated. Constant and sharp $T_{c,onset}$ on the transport resistance and specific heat capacity (C/T) strongly suggest that intragranular 1144 stoichiometric structures were not disturbed by a long period (~4 weeks) of the ambient air exposure. Atomic resolution analytical electron microscopy confirmed this scenario. Surface and cross-sectional microstructure analysis clearly exhibits that oxidization appeared at the grain boundaries, which is concentrated around open porosities. These results indicate that the boundaries between aggregates or intrinsic grains of the polycrystalline 1144 FBS compounds play a role as a percolative path for preferential oxygen diffusion. Such oxidization leads to suppression of intergranular superconducting transport currents of the 1144 phase.

5. References

[1] Yoichi Kamihara, Takumi Watanabe, Masahiro Hirano, and Hideo Hosono "Iron-Based Layered Superconductor La[$O_{1-x}F_x$]FeAs (x = 0.05−0.12) with T_c = 26 K" *Journal of the American Chemical Society* 2008 130 (11), 3296-3297, doi: 10.1021/ja800073m

[2] Hideo Hosono, Kazuhiko Kuroki, "Iron-based superconductors: Current status of materials and pairing mechanism" *Physica C: Superconductivity and its Applications*, Volume 514, 2015, Pages 399-422, ISSN 0921-4534, https://doi.org/10.1016/j.physc.2015.02.020.

[3] Lance Cooley, David Larbalestier, Kathleen Amm, "Challenges and opportunities to assure future manufacturing of magnet conductors for the accelerator sector" arXiv:2208.12379

[4] Chao Yao, "Fabrication and Properties of High-Performance 122-Type Iron-Based Superconducting Wires and Tapes", Springer, 2022.

[5] Xianping Zhang, Yanwei Ma, "Progress in the development of the 122-type IBS wires", Superconductivity, Volume 2, 2022, 100010, ISSN 2772-8307, https://doi.org/10.1016/j.supcon.2022.100010.

[6] C Pak, Y F Su, Y Collantes, C Tarantini, E E Hellstrom, D C Larbalestier and F Kametani, "Synthesis routes to eliminate oxide impurity segregation and their influence on intergrain connectivity in K-doped $BaFe_2As_2$ polycrystalline bulks" 2020 *Supercond. Sci. Technol.* 33 084010, DOI: 10.1088/1361-6668/aba01a

[7] C Yao, Y Ma, "Recent breakthrough development in iron-based superconducting wires for practical applications" Supercond. Sci. Technol. 32 023002 (2019)

[8] A Iyo, K. Kawashima, T. Kinjo, T. Nishio, S. Ishida, H. Fujihisa, Y. Gotoh, K. Kihou, H. Eisaki, Y. Yoshida, "New-Structure-Type Fe-Based Superconductors: Ca A Fe 4 As 4 (A = K, Rb, Cs) and Sr A Fe 4 As 4 (A = Rb, Cs)" *Journal of the American Chemical Society* 2016, *138* (10), 3410–3415. https://doi.org/10.1021/jacs.5b12571.

[9] A. Ichinose, S. Pyon, T. Tamegai, S. Ishida, "Elucidating the Origin of Planar Defects That Enhance Critical Current Density in CaKFe 4 As 4 Single Crystals" *Supercond Sci Technol* 2021, *34* (3), 034003. https://doi.org/10.1088/1361-6668/abdba7.

[10] A. Masi, A Angrisani, G. Celentano, A. La Barbera, A. Rufoloni, E. Silva, A. Vannozzi, F. Varsano, "Mechanochemically Assisted Low Temperature Synthesis Route of the 1144 Ca-K Iron Based Superconductor". *Supercond Sci Technol* 2020, *33* (7), 074003. https://doi.org/10.1088/1361-6668/ab9029.

[11] Z-H Sung, A. Duchenko, G. Celentano, J-Y Lee, X. Hu, N. Pompeo, F. Varsano, A. Masi, "Oxidation in Ca/K-1144 iron-based superconductors polycrystalline compounds", Superconductivity, Volume 8, 2023, 100062, ISSN 2772-8307, https://doi.org/10.1016/j.supcon.2023.100062.

[12] C. Tu, C. Dong, C. Fu, M. Han, M. Tang, H. Huang, C. Yao, D. Wang, X. Zhang, Y. Ma, "Origin and elimination of excess iron particles in off-stoichiometric Ba0.6K0.5-βFe2As2+δ superconductors", Scripta Materialia, Volume 235, 2023, 115595, ISSN 1359-6462, https://doi.org/10.1016/j.scriptamat.2023.115595.

[13] Z. Cheng, C. Dong, H. Yang, Q. Zhang, S. Awaji, L. Gu, H. Wen, Y. Ma, "Strengthened proximity effect at grain boundaries to enhance inter-grain supercurrent in Ba1-xKxFe2As2 superconductors", Materials Today Physics, Volume 28, 2022, 100848, ISSN 2542-5293, https://doi.org/10.1016/j.mtphys.2022.100848.

Acknowledgments

This material is based on work supported by the U.S. Department of Energy, Office of Science, Applied Physics and Superconducting –Technology Division, and LDRD 2020.007 Project.